Dalton Transactions

PAPER

View Article Online
View Journal

Cite this: DOI: 10.1039/c7dt04774f

Synthesis, characterization and derivatization of hydroxyl-functionalized iron(II) bis(NHC) complexes†

Anja C. Lindhorst,‡[a] Manuel Kaspar,‡[a] Philipp J. Altmann,[b] Alexander Pöthig[b] and Fritz E. Kühn*[a]

Received 18th December 2017,
Accepted 4th January 2018

DOI: 10.1039/c7dt04774f

rsc.li/dalton

The syntheses of a novel hydroxyl-functionalized tetradentate NHC/pyridine hybrid ligand and the corresponding Ag(I) and Fe(II) complexes are presented. Spectroscopic and X-ray diffraction techniques are used for structural investigations and cyclic voltammetry measurements reveal interesting electronic properties. Transmetalation of the trinuclear Ag(I) complex (**C1**) yields a mononuclear and a dinuclear iron(II) bis(NHC) complex (**C2** and **C3**), which can be separated by stepwise precipitation. The former is isostructural to iron(II) bis(NHC) complex **A**, which is a versatile oxidation catalyst. Furthermore, suitable conditions for esterification reactions of the ligand precursor and iron(II) bis(NHC) complex (**C2**) have been established, demonstrating the utility of the hydroxyl functionality for immobilization and derivatization purposes.

1. Introduction

N-Heterocyclic carbenes (NHC) have become an important ligand class in organometallic chemistry due to their high flexibility in terms of steric and electronic properties, particularly since the first catalytic applications of transition metal NHC complexes were reported in the 1990s.[1–6] Transition metal NHC complexes bearing multidentate ligand scaffolds with methylene-bridged NHC units are particularly stable due to the stabilizing chelate effect and the formation of a six-membered metallacycle.[7–9] Moreover, in addition to the wingtips and imidazolium backbone, bridging units offer an additional site for the modification of NHC ligands. Specifically designed functional groups can, for example, alter the solubility of transition metal NHC complexes, be used as anchoring sites for immobilization or for the extension of the ligand structure by further donor moieties or even metal centers.[7–10] In contrast to wingtip and backbone modifications, the number of reports on bridge-functionalized bis(NHC) ligands is limited.[11–14] For instance, our group reported a series of hydroxyl-functionalized bis(NHC) ligands with a variety of different wingtips. The corresponding palladium complexes could be successfully immobilized *via* the hydroxyl group and applied as catalysts for Suzuki–Miyaura reactions.[15,16] Moreover, coinage metal complexes of these ligands were isolated showing antiproliferative effects on cancer cell lines.[17] Recently, Hölscher and coworkers described a carboxylate-functionalized bis(NHC) iridium complex, which is water-soluble and catalyzes the hydrogenation of CO_2 to formate.[18]

In the context of catalytic applications, iron NHC complexes have gained increasing interest in the past two decades and could successfully be applied as catalysts in various homogeneous reactions including C–C couplings, reductions and oxidations.[19,20] Iron(II) complex **A** for example, bearing a methylene-bridged bis(NHC/pyridine) ligand, proved to be catalytically active in the oxidation of alkenes and arenes, olefin epoxidation as well as aldehyde olefination reactions (Fig. 1).[21–25]

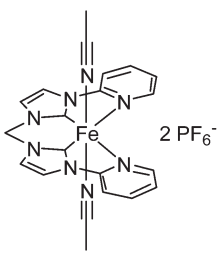

A

Fig. 1 Iron(II) bis(NHC) complex **A** is a potent catalyst for the oxidation of alkenes and arenes, olefin epoxidation as well as aldehyde olefination reactions.[21–25]

[a]*Molecular Catalysis, Catalysis Research Center and Department of Chemistry, Technical University of Munich, Lichtenbergstr. 4, D-85747 Garching bei München, Germany. E-mail: fritz.kuehn@ch.tum.de; Fax: (+49)-89-289-13247; Tel: (+49)-89-289-13096*

[b]*Catalysis Research Center and Department of Chemistry, Technical University of Munich, Lichtenbergstr. 4, D-85747 Garching bei München, Germany*

† Electronic supplementary information (ESI) available. CCDC 1811950–1811954. For ESI and crystallographic data in CIF or other electronic format see DOI: 10.1039/c7dt04774f

‡ These authors contributed equally to this work.

However, especially under oxidizing conditions, catalyst degradation is a serious issue and strategies towards higher durability are to be explored. Potentially, this could be achieved by altering the coordination environment of the iron center with particular focus in the trans-labile coordination sites to prevent unselective interactions with, *e.g.*, radicals. Immobilization of molecular complexes or the introduction of additional, reversibly coordinating donor moieties may therefore benefit the catalytic performance and can be realized *via* suitable functionalization of the tetradentate ligand.[10] Furthermore, synthesis of a heterogenized analogue of iron NHC complex **A** could help to elucidate the fate of the catalytically active species as a spacial separation of the reactive sites should translate into a higher turnover number if a bimolecular degradation pathway is present.

In this work, the synthesis and characterization of 1,1′-(2-hydroxyethane-1,1-diyl) bridge-functionalized silver and iron bis(NHC) complexes are reported. Performing esterification reactions, the utility of the hydroxyl group as a versatile target for the derivatization of the bis(imidazolium) salt itself and the corresponding mononuclear iron NHC complex is demonstrated.

2. Results and discussion

2.1. Synthesis of a hydroxyl-functionalized ligand precursor

In order to introduce a suitable functional group for derivatization and immobilization purposes to iron NHC complex **A**, bridge-functionalized bis(imidazolium) salt **P1** was synthesized in a nucleophilic substitution reaction from 2,2-dibromoethanol and 2-(imidazol-1-yl)pyridine in analogy to literature-known procedures.[15–17] Due to the low nucleophilicity of the pyridine-substituted imidazole, no reaction was observed using 2,2-dichloroethanol as a substrate. Instead, the more reactive 2,2-dibromoethanol has to be employed as well as a high reaction temperature of 130 °C. However, the enhanced elimination of HBr from 2,2-dibromoethanol under these conditions results in a moderate overall yield of 39% after anion exchange with NH_4PF_6.

2.2. Synthesis and characterization of hydroxyl-functionalized iron(II) NHC complexes

There is a variety of different approaches, allowing access to iron NHC complexes.[19] Unlike the reported synthesis of iron(II) complex **A**,[26] aminolysis of iron(II) bis(trimethylsilyl)amide $[Fe\{N(SiMe_3)_2\}_2(THF)]$ with the bis(imidazolium) salt **P1** (see Scheme 1) yielded no product. This may be attributed to the presence of the hydroxyl group, which presumably reacts with one of the internal base equivalents and subsequently may form a stable iron-oxo bond. Alternatively, transmetalation of silver NHC complexes with iron halides has been reported as an access route to iron NHC compounds.[27–29] In line of this, silver NHC complex **C1** was synthesized from **P1** and silver(I) oxide with 84% yield (Scheme 2). ^{1}H NMR spectra in solution reveal all expected signals of the ligand molecules and the splitting pattern suggests a symmetric coordination mode (*cf.* ESI-MS, Fig. S7†). The characteristic signals of the carbene carbon atoms in $^{13}C\{^1H\}$ spectra are found at 183.67 ppm, which is consistent with previously reported Ag complexes bearing NHC/pyridine hybrid ligands.[30,31]

Single crystals suitable for X-ray diffraction were obtained by slow diffusion of diethyl ether into an acetonitrile solution of **C1**. Similarly to the structure of the silver(I) complex bearing the analogous un-functionalized NHC/pyridine hybrid ligand,[30] three silver ions are coordinated by two ligand molecules (Fig. 2). Two of the silver atoms are coordinated almost linearly by the carbene moieties (bond angles of 175.5(5)° and 177.6(5)°) and the third one is bound to two pyridine units and two acetonitrile molecules. The Ag–C_{NHC} distances range between 2.089(13) and 2.105(13) Å corresponding well to previously reported silver–NHC bond distances.[32] The three silver

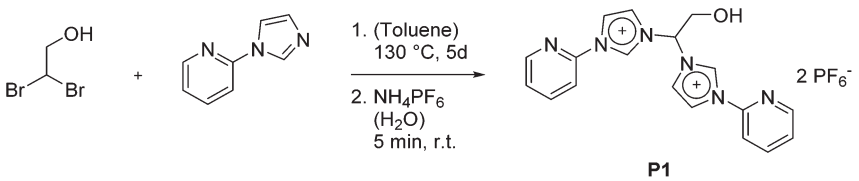

Scheme 1 Synthesis of bis(imidazolium) salt **P1**.

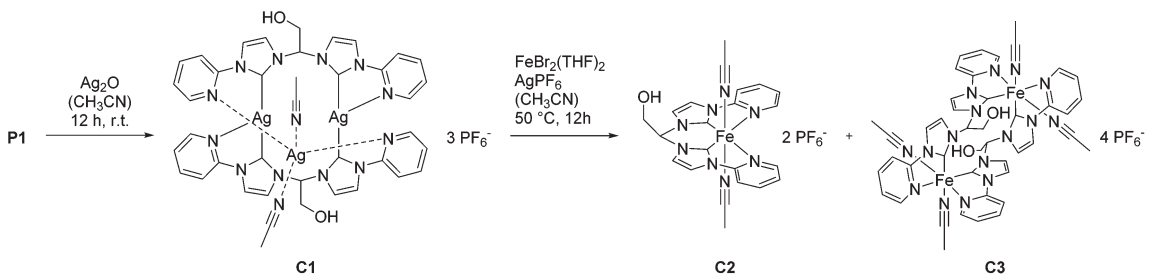

Scheme 2 Synthesis of silver and iron bis(NHC) complexes bearing a pendant hydroxyl group.

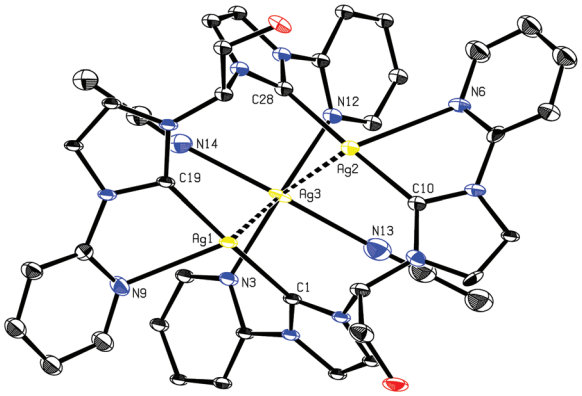

Fig. 2 ORTEP style representation of the cationic fragment of **C1** with ellipsoids shown at the 50% probability level. Hydrogen atoms, cocrystallized solvent molecules, and counter ions are omitted for clarity. Selected geometrical parameters: Ag1–Ag3 2.9153(14) Å, Ag2–Ag3 2.9024(14) Å, Ag1–C1 2.089(13) Å, Ag1–C19 2.105(13) Å, Ag3–N3 2.348(11) Å, Ag3–N12 2.385(11) Å, Ag3–N13 2.611(14) Å, Ag3–N14 2.585(14) Å, C1–Ag1–C19 177.6(5)°, C10–Ag2–C28 175.5(5)°, N3–Ag3–N12 137.7(3)°.

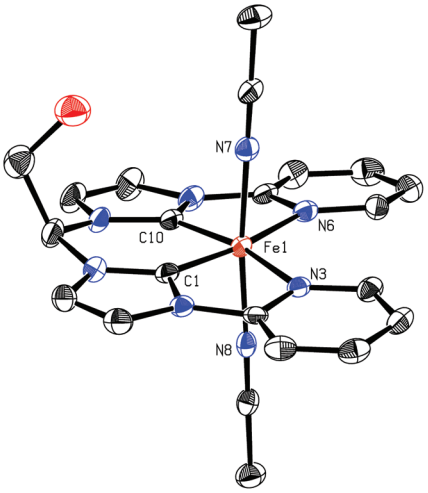

Fig. 3 ORTEP style representation of the cationic fragment of **C2** with ellipsoids shown at the 50% probability level. Hydrogen atoms, cocrystallized solvent molecules, and counter ions are omitted for clarity. Selected geometrical parameters: Fe1–C1 1.826(4) Å, Fe1–C10 1.833(4) Å, Fe1–N7 1.913(4) Å, Fe1–N8 1.923(4) Å, Fe1–N3 2.082(3) Å, Fe1–N6 2.104(4) Å, Fe1–O1 4.061(4) Å, N7–Fe1–N8 173.99(15)°.

atoms form a triangle and the rather short Ag1–Ag3 and Ag2–Ag3 distances of 2.9153(14) Å and 2.9024(14) Å suggest argentophilic interactions.[32]

Transmetalation of **C1** with $FeBr_2(THF)_2$ at room temperature affords a mixture of the expected mononuclear iron(II) complex **C2** and a dinuclear iron(II) complex **C3** in almost equal amounts (Scheme 2). To balance the stoichiometry an additional equivalent of $AgPF_6$ is added during the reaction. By increasing the reaction temperature to 50 °C, the ratio of the two product complexes can be shifted in favor of the mononuclear complex **C2** (**C2** : **C3** 2 : 1). The two complexes, which are both air-stable, can be separated by stepwise addition of diethyl ether to the acetonitrile solution. As the dinuclear complex **C3** is less soluble, it precipitates first and can be collected by filtration. Further addition of diethyl ether affords **C2** as a red solid.

The monomeric structure of **C2** was proven by ESI-MS techniques and ^{1}H NMR spectroscopic investigations confirm the equatorial coordination geometry of the tetradentate ligand as only one set of signals is present corresponding to the pyridine and imidazolylidene units (*cf.* ESI-MS, Fig. S10†). The $^{13}C\{^1H\}$ signals of the carbenic carbon atoms appear at a chemical shift of 217.06 ppm and lie in the range of previously reported iron(II) NHC complexes.[19,20] X-ray diffraction measurements of single crystals obtained by slow diffusion of diethyl ether into an acetonitrile solution reveal the structural similarity of **C2** to the un-functionalized complex **A** (Fig. 3).[26] **C2** exhibits a distorted octahedral coordination geometry bearing two axially coordinating acetonitrile molecules and the tetradentate NHC/pyridine hybrid ligand covering the equatorial positions. The Fe–C_{NHC} bond distances of 1.826(4) and 1.833(4) Å are close to those of complex **A** as are the Fe–N_{Py} distances of 2.082(3) and 2.104(4) Å and the Fe–N_{MeCN} distances (1.913(4) and 1.923(4) Å). The hydroxymethyl group is pointing outwards of the equatorial coordination plane and no iron–oxygen interaction is observed (distance Fe1–O1 4.061(4) Å). These data confirm that complex **C2** is isostructural to **A** and that a hydroxyl-functionalization of the ligand methylene bridge does not have any major influence on the coordination geometry.

In contrast, complex **C3**, which is formed simultaneously with **C2** in the transmetalation reaction, possesses a dinuclear structure as indicated by ESI-MS. ^{1}H NMR spectra in solution further reveal that the symmetry of the coordination of the tetradentate ligand is broken as for each proton of the pyridine and imidazolylidene units a separate signal can be observed (*cf.* ESI-MS, Fig. S13†). Interestingly, the proton signal corresponding to the methylene group adjacent to the hydroxyl group is split into two independent signals indicating that the two CH_2 protons are diastereotopic in this complex. $^{13}C\{^1H\}$ NMR spectra of **C3** in solution exhibit two signals corresponding to the carbenic carbon atoms at 209.92 and 200.85 ppm, respectively. The structure could be further confirmed by X-ray diffraction of single crystals obtained by slow diffusion of diethyl ether into a solution of **C3** in acetonitrile (Fig. 4). It shows that each of the NHC/pyridine units of the tetradentate ligand coordinates to a different iron atom thus bridging the two metal centers and creating a distorted octahedral coordination geometry, which is completed by two *cis*-coordinated acetonitrile ligands. The two NHC/pyridine units of each ligand molecule are twisted against each other with a torsion angle of 87.70°. The Fe–C_{NHC} bond distances amount to 1.9209(18) and 1.9333(18) Å and are thus slightly longer compared to complex **C2**, yet still lie in the range of previously reported iron NHC complexes.[19,20] Likewise complex **C2**, the hydroxymethyl groups bound to the ligand methylene bridge are directed away from the iron centers and no iron–oxygen interactions are observed.

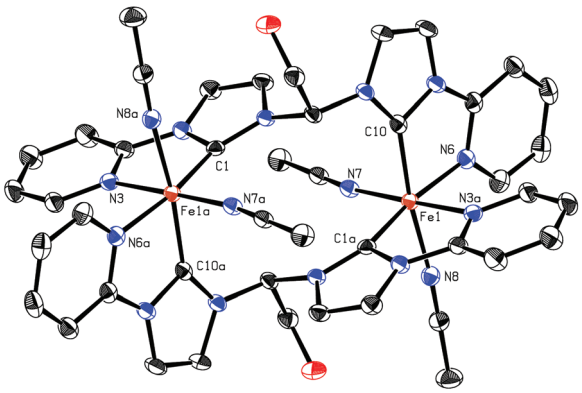

Fig. 4 ORTEP style representation of the cationic fragment of **C3** with ellipsoids shown at the 50% probability level. Hydrogen atoms, cocrystallized solvent molecules, and counter ions are omitted for clarity. Selected geometrical parameters: Fe1–C10 1.9209(18) Å, Fe1–N6 2.0183(5) Å, Fe1–C1a 1.9333(18) Å, Fe1–N3a 1.9996(15) Å, Fe1–N7 1.9299(15) Å, Fe1–N8 1.9676(16) Å.

2.3. Esterification of hydroxyl-functionalized ligand precursor P1 and iron(II) NHC complex C2

In analogy to literature-known NHC ligand precursors,[10,12,13,18] the hydroxyl functionality of **P1** may serve as a site for further functionalization of the ligand scaffold or as an anchoring site for immobilization approaches. Therefore, esterification reactions of both ligand precursor **P1** and the functionalized iron(II) NHC complex **C2** were performed to demonstrate the feasibility of such reactions and identify suitable reaction conditions (Scheme 3).

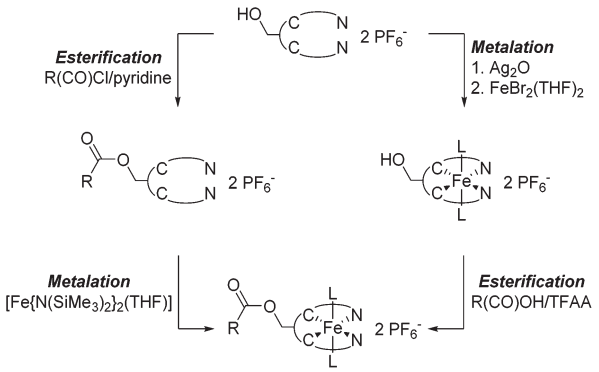

Scheme 3 Strategies towards the synthesis of esterified iron(II) NHC complexes. The tetradentate NHC/pyridine hybrid ligand **P1** is depicted schematically.

Esterification reactions with ligand precursor **P1** were performed using hexanoyl, benzoyl and nicotinoyl chloride to demonstrate the feasibility of such reactions with alkylic, aromatic and heteroaromatic organic acids (Scheme 4). With acetonitrile as solvent and in the presence of pyridine as base, the reactions proceed smoothly at room temperature within 12–21 h depending on the acid chloride used. After workup and repeated anion exchange with NH_4PF_6 **P2a–P2c** are obtained in yields of 44–82%. The reaction process can be followed by ^{1}H NMR as the signal of the hydroxyl proton at 6.26 ppm disappears and the signals corresponding to the CH_2 protons adjacent to the hydroxyl group show a distinct downfield shift from 4.55 ppm for **P1** to 5.21, 5.44, and 5.44 ppm for **P2a**, **P2b**, and **P2c** as the reaction proceeds. The same accounts for signal of the bridging NC*H*CH_2 proton, which is shifted downfield from 7.18 ppm to 7.53, 7.70, and 7.67 ppm for **P2a**, **P2b**, and **P2c**. Only minor changes of the chemical shifts of all other signals are observed by ^{1}H NMR.

In accordance to the strategy presented by Danopoulos *et al.*[33] the esterified ligand precursors **P2a–P2c** can be converted to the corresponding complexes **C2a–C2c** in good yields between 52 and 76% by aminolysis with iron(II) bis(trimethylsilyl)amide (Scheme 4). The product complexes have been characterized by NMR spectroscopy, ESI-MS and elemental analysis. The data suggest a monomeric structure in each case with the iron center being coordinated in a distorted octahedral geometry analogous to the structures of **C2** and **A**. Similar to the ligand precursors **P2a–P2c** in the ^{1}H NMR spectra of **C2a–C2c** the chemical shift of the CH_2 proton signals is moved downfield upon esterification. For the hydroxyl-functionalized complex **C2** the signal is observed at 4.19 ppm, while it is found at 4.60, 4.83, and 4.78 ppm for **C2a**, **C2b**, and **C2c**, respectively. The signal of the adjacent NC*H*CH_2 proton is similarly shifted downfield compared to complex **C2** (7.28 ppm (**C2**) to 7.43 (**C2a**), 7.59 (**C2b**), and 7.58 ppm (**C2c**)).

Alternatively to ligand precursor **P2**, iron(II) complex **C2** can also be used as a substrate for esterification reactions. This is

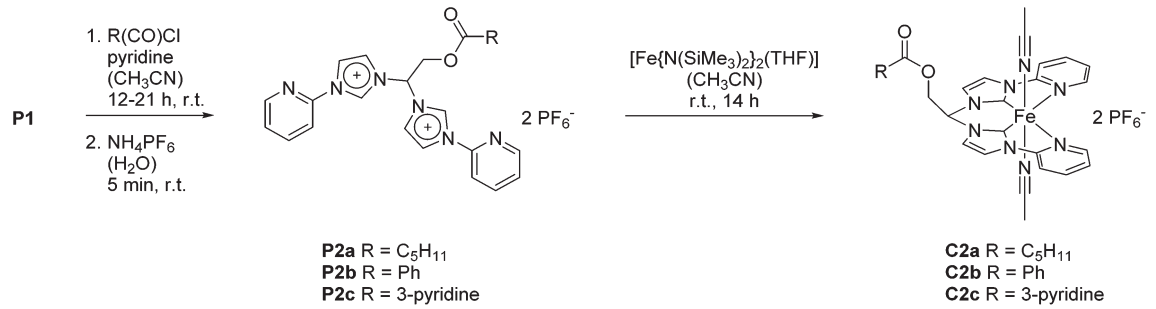

Scheme 4 Esterification reactions of bis(imidazolium) salt **P1** with various acid chlorides and subsequent synthesis of iron(II) NHC complexes.

especially important in the context of catalyst immobilization as often the precise characterization of heterogenized metal complexes poses difficulties and by grafting a defined metal complex in the last synthetic step, *e.g. via* an esterification reaction, characterization can be facilitated and incomplete metalation avoided.[10,34] However, acid chlorides were found to be inapplicable as no products could be isolated and degradation of **C2** was observed. On the other hand, organic acid anhydrides, which have been used before as mild derivatization reagents for NHC complexes,[35] proved to be suitable reagents to realize such reactions (Scheme 5). Depending on the reactivity of the organic acid two different methods can be applied: one possibility is reacting the organic acid with trifluoroacetic anhydride (TFAA) to form a mixed anhydride, which is subsequently added to a solution of **C2** leading to the formation of the esterified complexes **C2a** and **C2b** (Method A). However, in case of nicotinic acid instead of the desired product **C2c**, complex **C2d** is formed bearing a trifluoroacetic ester group. In comparison to hexanoic and benzoic acid (pK_a: 4.48 (hexanoic acid), 4.20 (benzoic acid)), nicotinic acid has a significantly lower pK_a of 2.03,[36,37] which is accompanied by a better stabilization of the corresponding carboxylate. Apparently, as the difference in pK_a between trifluoroacetic acid (pK_a: 0.23)[36] and the respective organic acid decreases, the reactivity of the mixed anhydride is affected significantly and the selectivity of the esterification reaction declines. As an alternative, **C2** can be reacted with nicotinic anhydride in the presence of diisopropylethylamine (DIPEA) as base yielding the desired complex **C2c** in 52% yield (Method B). This method is also applicable to benzoic anhydride and complex **C2b** is obtained in 48% yield. The product yields achieved applying method B are lower compared to method A. This observation can be attributed to the necessity of using a base to initiate the reaction. In this context, the reaction time is an important parameter as, despite the high steric demand of DIPEA, slow degradation of **C2** is observed in its presence.

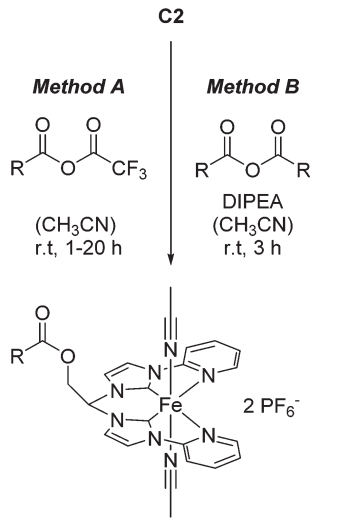

C2a R = C_5H_{11} (***A*** 77%)
C2b R = Ph (***A*** 99%, ***B*** 48%)
C2c R = 3-pyridine (***B*** 52%)
C2d R = CF_3 (***A*** 99%)

Scheme 5 Esterification of iron(II) complex **C2** by organic acid anhydrides.

Single crystals suitable for X-ray diffraction measurements of **C2a** and **C2b** have been obtained by slow diffusion of diethyl ether into an acetonitrile solution of the respective complexes. As Fig. 5 reveals, both complexes are isostructural to **C2** and **A** as the iron center is coordinated in a distorted octahedral fashion by the tetradentate NHC/pyridine hybrid ligand and two apical acetonitrile molecules. Again, no inter-

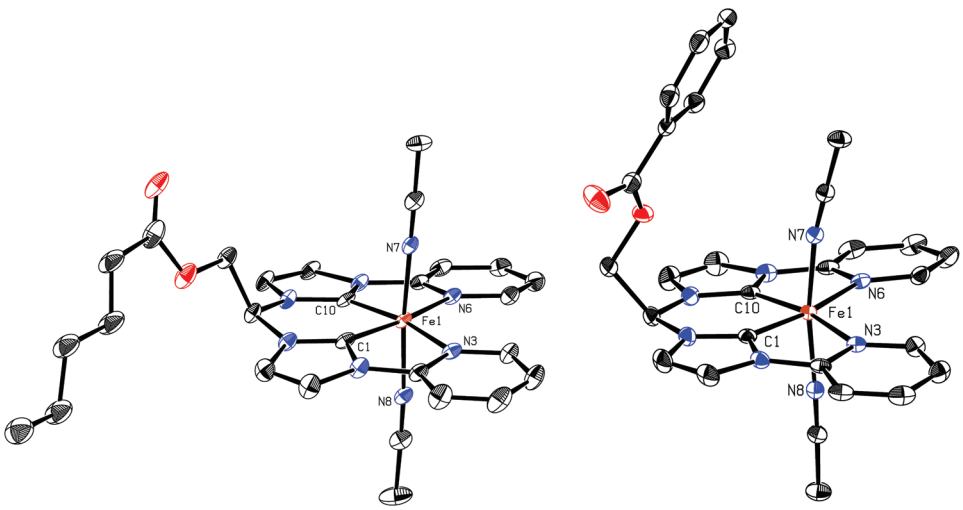

Fig. 5 ORTEP style representation of the cationic fragments of **C2a** and **C2b** with ellipsoids shown at the 50% probability level. Hydrogen atoms, cocrystallized solvent molecules, and counter ions are omitted for clarity. Selected geometrical parameters: C2a Fe1–C1 1.835(5) Å, Fe1–C10 1.833(4) Å, Fe1–N7 1.910(4) Å, Fe1–N8 1.924(4) Å, Fe1–N3 2.091(4) Å, Fe1–N6 2.077(4) Å, N7–Fe1–N8 175.16(16)°. C2b Fe1–C1 1.830(2) Å, Fe1–C10 1.829(2) Å, Fe1–N7 1.9212(18) Å, Fe1–N8 1.9252(18) Å, Fe1–N3 2.0863(18) Å, Fe1–N6 2.0798(19) Å, N7–Fe1–N8 171.26(7)°.

action of the functional group attached to the ligand backbone, in this case ester groups, and the metal center were observed. Compared to both **C2** and **A** the distances between the iron atoms and the coordinating atoms remain nearly unchanged for **C2a** and **C2b**.

2.4. Electrochemical characterization

To evaluate the influence of the methylene bridge functionalization of complex **A** with hydroxymethyl and ester groups on the electronic properties of the iron center, cyclic voltammetry (CV) measurements in acetonitrile solution were performed. Complexes **C2** and **C2a–C2d** show a one-electron redox process, which can be assigned to the Fe(II)/Fe(III) redox couple (Fig. 6). The half-wave potentials $E_{1/2}$ *vs.* Fc/Fc^+ are 427 mV for **C2**, 478 mV for **C2a**, 480 mV for **C2b**, 490 mV for **C2c**, and 502 mV for **C2d** and the oxidation proved to be fully reversible for all complexes for at least 20 cycles. The peak separation ΔE of 74 mV to 82 mV lies within the typical range for a reversible one-electron process and corresponds well to previously described, related iron complexes.[38–42] The half-wave potential of **C2** deviates only marginally from the reported potential of the un-functionalized complex **A** of 423 mV *vs.* Fc/Fc^+.[26] Taking into account the structural data presented above, this indicates that the functionalization of the ligand backbone with a hydroxymethyl group has no significant influence on the electronic situation of the iron center. Furthermore, the required potentials for the oxidation of the esterified complexes **C2a–C2d** are 50–70 mV higher, which can be attributed to the electron withdrawing properties of the ester groups. As the electron density at the iron center is decreased, a higher half-wave potential is observed. Within the series of **C2a** to **C2d**, the variation of the acid substituents has little influence on the half-wave potentials, which increase slightly with the acid strength. However, compared to the effect of axial substitution reactions with phosphine-, pyridine- or isocyanide-based ligands on the electronic properties of **A**,[40,43] the observed changes in the half-wave potentials upon ester-functionalization of the ligand methylene bridge are small.

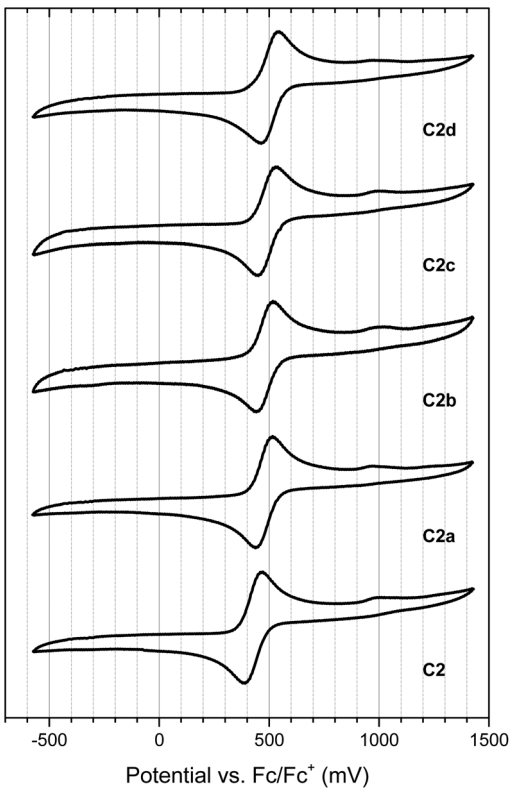

Fig. 6 Cyclic voltammograms of complexes **C2** and **C2a–C2d**. Half-wave potentials are determined to $E_{1/2}$ = 427 mV (**C2**), 478 mV (**C2a**), 480 mV (**C2b**), 490 mV (**C2c**), and 502 mV (**C2d**). All potentials are referenced to the half-wave potential of the Fc/Fc^+ redox couple.

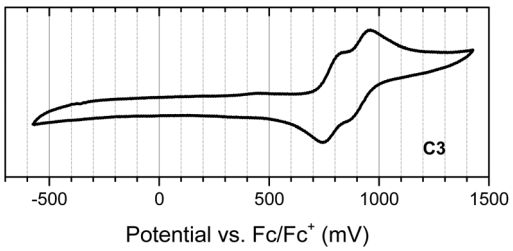

Fig. 7 Cyclic voltammogram of dinuclear complex **C3**. The half-wave potentials are determined to $E_{1/2}$ = 793 mV and 912 mV. All potentials are referenced to the half-wave potential of the Fc/Fc^+ redox couple.

The CV data of diiron complex **C3** reveals two reversible waves at $E_{1/2}$ = 793 mV and 912 mV (Fig. 7). The separation of the two oxidation events amounts to 119 mV, indicating weak electronic coupling between the two metal centers.[44–46] However, as charge delocalization through the ligand is unlikely due to the saturated nature of the bridge between the two NHC/pyridine units, the peak splitting in the CV data must result from a through-space electrostatic interaction.[47]

3. Conclusions

The synthesis and characterization of a new 1,1′-(2-hydroxyethane-1,1-diyl) bridge-functionalized bis(imidazolium) salt has been presented providing access to tunable silver and iron bis(NHC) complexes. In addition to the targeted mononuclear analogue of iron(II) NHC complex **A**, a dinuclear iron complex was synthesized displaying interesting structural features and a weak electronic coupling of the two iron centers. Performing esterification reactions and determining suitable reaction conditions, the utility of the hydroxyl group as a versatile platform for the derivatization of the ligand precursor on the one hand and the corresponding mononuclear iron NHC complex on the other hand has been demonstrated. Thus, four iron(II) bis(NHC) complexes bearing aliphatic, aromatic or heteroaromatic ester groups could be isolated and fully characterized. These reactions serve as model reactions for the design of extended ligand scaffolds and lay the foundations for the immobilization of molecular iron NHC complexes analogous

complex **A**, which is an active catalyst in a wide range of reactions. Experiments following these strategies are currently ongoing. Moreover, the presented iron NHC complexes are to be used as catalysts in oxidation reactions in order to evaluate the influence of the ligand functionalization on their catalytic behavior in comparison to complex **A**.

4. Experimental section

4.1. General remarks

All chemicals were purchased from commercial suppliers and used without further purification. Anhydrous solvents were obtained from an MBraun solvent purification system and degassed by freeze–pump–thaw techniques. All syntheses were performed under standard Schlenk conditions unless stated otherwise. 2-(Imidazol-1-yl)pyridine[48] and iron(II) bis(trimethylsilyl)amide[49] were synthesized according to previously published procedures. Liquid NMR spectra were recorded on Bruker Avance DPX 400 and Bruker CRX 400 spectrometers. Chemical shifts are provided in parts per million (ppm) and spectra were referenced using the residual solvent shifts as internal standards ($CDCl_3$, ^1H δ 7.26, DMSO-d_6, ^1H δ 2.50, ^{13}C δ 39.52, CD_3CN, ^1H δ 1.94, ^{13}C δ 118.26). Elemental analyses were performed by the microanalytical laboratory of TUM and a Thermo Scientific LCQ/Fleet spectrometer was employed to obtain ESI-MS data.

A Metrohm Autolab PGSTAT302N potentiostat was used together with the Nova 1.11 software for cyclic voltammetry measurements. A graphite electrode was chosen as counter electrode, together with platinum as working electrode and Ag/$AgNO_3$ (0.01 M in acetonitrile with 0.1 M tetrabutylammonium hexafluorophosphate) as reference electrode. For all measurements, 2.0–3.0 mg of the respective compound were dissolved in 1.0 mL of a 0.1 M solution of tetrabutylammonium hexafluorophosphate in acetonitrile under inert conditions. The potential was scanned with 100 mV s^{-1} and the obtained values were referenced against the Fc/Fc^+ redox couple as internal standard (0.48 V *versus* SCE).[50]

4.2. Single-crystal X-ray diffraction

The X-ray intensity data of **C1–C3** were collected on an X-ray single crystal diffractometer equipped with a CCD detector, a Mo fine-focus tube with MoK_α radiation (λ = 0.71073 Å) and a graphite monochromator by using the APEX II software package.[51] The X-ray intensity data of **C2a** were collected on an X-ray single crystal diffractometer equipped with a CMOS detector (Bruker Photon-100), an IMS microsource with MoK_α radiation (λ = 0.71073 Å) and a Helios mirror optic by using the APEX III software package.[52] The X-ray intensity data of **C2b** were collected on an X-ray single crystal diffractometer equipped with a CMOS detector (Bruker Photon-100), a rotating anode (Bruker TXS) with MoK_α radiation (λ = 0.71073 Å) and a Helios mirror optic by using the APEX III software package.[52] The measurements were performed on single crystals coated with perfluorinated ether. The crystals were fixed on the top of a microsampler, transferred to the diffractometer and frozen under a stream of cold nitrogen. A matrix scan was used to determine the initial lattice parameters. Reflections were corrected for Lorenz and polarization effects, scan speed, and background using SAINT.[53] Absorption corrections, including odd and even ordered spherical harmonics were performed using SADABS.[53] Space group assignments were based upon systematic absences, E statistics, and successful refinement of the structures. Structures were solved by direct methods with the aid of successive difference Fourier maps, and were refined against all data using the APEX III software in conjunction with SHELXL-2014[54] and SHELXLE.[55] H atoms bound to oxygen atoms were allowed to refine freely with an O–H distance of 0.84 Å. Other H atoms were placed in calculated positions and refined using a riding model, with methylene and aromatic C–H distances of 0.99 and 0.95 Å, respectively, and $U_{iso}(H) = 1.2U_{eq}(C)$. Full-matrix least-squares refinements were carried out by minimizing $\Delta w(F_o^2 - F_c^2)^2$ with SHELXL-97[56] weighting scheme. Neutral atom scattering factors for all atoms and anomalous dispersion corrections for the non-hydrogen atoms were taken from International Tables for Crystallography.[57] The image of the crystal structure was generated by PLATON.[58] CCDC 1811950–1811954† contains the supplementary data for the structures.

4.3. Syntheses

4.3.1. 2,2-Dibromoethanol. In a three-necked flask equipped with a dropping funnel and a reflux condenser $LiAlH_4$ (4.35 g, 114.8 mmol, 2.0 eq.) is suspended in diethyl ether (80 mL). At 0 °C a solution of 2,2-dibromoacetic acid (12.5 g, 57.4 mmol, 1.0 eq.) in diethyl ether (25 mL) is added dropwise. After completion of the addition the reaction mixture is stirred at room temperature for 2.5 h. Subsequently excess $LiAlH_4$ is quenched by slowly adding H_2O (30 mL) under ice cooling followed by addition of aqueous H_2SO_4 (100 mL, 10% w/w). After separation of the organic phase, the aqueous phase is extracted with diethyl ether (3 × 50 mL). The combined organic phases are washed with saturated $NaHCO_3$ solution (50 mL) and H_2O (50 mL), dried over $MgSO_4$ and the solvent is removed *in vacuo* yielding 2,2-dibromoethanol (5.18 g, 25.4 mmol, 44% yield) as a colorless oil.

^1H NMR (400.13 MHz, 295.1 K, $CDCl_3$): δ 5.66 (t, J = 5.9 Hz, 1H, C*H*), 4.04 (dd, J = 7.1, 5.9 Hz, 2H, CH_2), 2.43 (t, J = 7.4 Hz, 1H, O*H*). $^{13}C\{^1H\}$ NMR (100.62 MHz, 295.5 K, $CDCl_3$): δ 70.0 (*C*H_2), 47.1 (*C*H).

4.3.2. Ligand precursor P1. In an ACE pressure tube 2,2-dibromoethanol (2.45 g, 12.0 mmol, 1.0 eq.) and 2-(imidazol-1-yl)pyridine (4.35 g, 30.0 mmol, 2.5 eq.) are dissolved in toluene (12 mL) in air. The tube is sealed tightly and heated to 130 °C for 5 days. After cooling to room temperature the brown precipitate is washed subsequently with acetonitrile, ethanol and dichloromethane (3 × 10 mL each). Recrystallization from methanol yields an off-white powder. The intermediate product is dissolved in water (5 mL) and added dropwise to a solution of ammonium hexafluorophosphate (1.96 g, 12.0 mmol, 1.0 eq.) in water (5 mL). The resulting white pre-

cipitate is washed carefully with water and dried *in vacuo* yielding imidazolium salt **P1** as a white solid (2.92 g, 4.68 mmol, 39%).

^{1}H NMR (400.13 MHz, 295.1 K, DMSO-d_6): δ 10.35 (t, J = 1.7 Hz, 2H, H_{Im}), 8.75–8.66 (m, 4H, H_{Im} + H_{Py}), 8.35–8.24 (m, 4H, H_{Im} + H_{Py}), 8.08 (d, J = 8.2 Hz, 2H, H_{Py}), 7.71 (dd, J = 7.5, 4.8 Hz, 2H, H_{Py}), 7.18 (t, J = 5.4 Hz, 1H, NC*H*CH$_2$), 6.26 (t, J = 5.7 Hz, 1H, O*H*), 4.55 (t, J = 5.5 Hz, 2H, NCHC*H*$_2$). ^{13}C{^{1}H} NMR (100.62 MHz, 295.5 K, DMSO-d_6): δ 149.89 (C_{Py}), 146.47 (C_{Py}), 141.34 (C_{Py}), 136.82 (N*C*HN$_{Im}$), 126.29 (C_{Py}), 123.03 (C_{Im}), 120.24 (C_{Im}), 114.94 (C_{Py}), 71.65 (N*C*HCH$_2$), 60.23 (NCH*C*H$_2$). MS-ESI (m/z): [**P1**–PF$_6$]$^+$ calcd: 479.12, found: 478.92; [**P1**–2PF$_6$]$^{2+}$ calcd: 167.08, found: 167.16. Anal. calcd for $C_{18}H_{18}F_{12}N_6OP_2$: C 34.63, H 2.91, N 13.46. Found: C 34.15, H 2.96, N 13.36.

4.3.3. Complex C1. In air **P1** (250.0 mg, 0.4 mmol, 1.0 eq.) is dissolved in acetonitrile (5 mL) and Ag_2O (278.1 mg, 1.2 mmol, 3.0 eq.) is added. The suspension is stirred at room temperature under light exclusion for 12 h. After filtration, diethyl ether is added slowly to the brown solution until it becomes colorless. It is decanted from the brown oil and the product is precipitated by further addition of diethyl ether. The precipitate is isolated and washed with diethyl ether yielding **C1** as a white solid (266.1 mg, 0.2 mmol, 84%).

^{1}H NMR (400.13 MHz, 295.1 K, CD_3CN): δ 7.91 (d, J = 2.1 Hz, 4H, H_{Im}), 7.88 (d, J = 4.7 Hz, 4H, H_{Py}), 7.86 (d, J = 2.0 Hz, 4H, H_{Im}), 7.82 (dt, J = 7.9, 1.8 Hz, 4H, H_{Py}), 7.65 (d, J = 8.1 Hz, 4H, H_{Py}), 7.32 (brs, 2H, NC*H*CH$_2$), 7.26 (dd, J = 6.9, 5.0 Hz, 4H, H_{Py}), 4.63 (t, J = 5.3 Hz, 4H, NCHC*H*$_2$), 4.01 (t, J = 5.2 Hz, 2H, O*H*). ^{13}C{^{1}H} NMR (100.62 MHz, 295.5 K, CD_3CN): δ 183.67 (C_{Im}), 150.78 (C_{Py}), 149.61 (C_{Py}), 141.12 (C_{Py}), 125.41 (C_{Py}), 122.33 (C_{Im}), 121.60 (C_{Im}), 116.45 (C_{Py}), 78.13 (N*C*HCH$_2$), 62.00 (NCH*C*H$_2$). Anal. calcd for $C_{40}H_{18}F_{38}Ag_3F_{18}N_{14}O_2P_3$: C 31.92, H 2.54, N 13.03. Found: C 31.05, H 2.39, N 12.09.

4.3.4. Complex C2. C1 (102.0 mg, 67.8 μmol, 1.0 eq.), $FeBr_2(THF)_2$ (48.8 mg, 135.6 μmol, 2.0 eq.) and silver(I) hexafluorophosphate (18.9 mg, 74.6 μmol, 1.1 eq.) are dissolved in acetonitrile (3 mL). The resulting solution is stirred under light exclusion at 50 °C for 12 h. After filtration, diethyl ether is cautiously added to the orange solution until an orange solid precipitates (complex **C3**). The solution is decanted and addition of further diethyl ether yields another orange precipitate, which is filtered off, washed with diethyl ether and dried *in vacuo*. **C2** is obtained as an orange solid in 40% yield (41.0 mg, 54.5 μmol).

^{1}H NMR (400.13 MHz, 295.1 K, CD_3CN): δ 9.57 (d, J = 4.9 Hz, 2H, H_{Py}), 8.35 (m, 2H, H_{Py}), 8.32 (d, J = 2.3 Hz, 2H, H_{Im}), 8.06 (d, J = 8.3 Hz, 2H, H_{Py}), 7.90 (d, J = 2.3 Hz, 2H, H_{Im}), 7.76 (ddd, J = 7.6, 5.4, 1.1 Hz, 2H, H_{Py}), 7.28 (t, J = 3.4 Hz, 1H, NC*H*CH$_2$), 4.19 (dd, J = 6.6, 3.4 Hz, 2H, NCHC*H*$_2$), 3.39 (t, J = 6.7 Hz, 1H, O*H*). ^{13}C{^{1}H} NMR (100.62 MHz, 295.5 K, CD_3CN): δ 217.06 (C_{Im}), 155.29 (C_{Py}), 153.74 (C_{Py}), 142.29 (C_{Py}), 125.99 (C_{Im}), 124.35 (C_{Py}), 120.19 (C_{Im}), 113.05 (C_{Py}), 76.94 (N*C*HCH$_2$), 66.39 (NCH*C*H$_2$). MS-ESI (m/z): [**C2**–2CH$_3$CN–2PF$_6$]$^{2+}$ calcd: 194.04, found: 194.23. Anal. calcd for $C_{22}H_{22}F_{12}FeN_8OP_2$: C 34.76, H 2.92, N 14.74. Found: C 34.39, H 2.85, N 14.27.

4.3.5. Complex C3. C1 (102.0 mg, 67.8 μmol, 1.0 eq.), $FeBr_2(THF)_2$ (48.8 mg, 135.6 μmol, 2.0 eq.) and silver(I) hexafluorophosphate (18.9 mg, 74.6 μmol, 1.1 eq.) are dissolved in acetonitrile (3 mL). The resulting solution is stirred under light exclusion at 50 °C for 12 h. After filtration, diethyl ether is cautiously added to the orange solution until an orange solid precipitates. The solution is decanted and the precipitate is washed with diethyl ether and dried *in vacuo*. The remaining solution still contains complex **C2**. **C3** is obtained as an orange solid in 41% yield (42.6 mg, 28.0 μmol).

^{1}H NMR (400.13 MHz, 295.1 K, CD_3CN): δ 9.30 (d, J = 5.6 Hz, 2H, H_{Py}), 8.56 (d, J = 2.4 Hz, 2H, H_{Im}), 8.53 (m, 2H, H_{Py}), 8.34 (d, J = 8.3 Hz, 2H, H_{Py}), 8.11 (m, 4H, $H_{Im'}$ + H_{Im}), 7.91–7.83 (m, 4H, H_{Py} + $H_{Py'}$), 7.63 (d, J = 8.2 Hz, 2H, $H_{Py'}$), 6.98 (ddd, J = 7.3, 5.9, 1.2 Hz, 2H, $H_{Py'}$), 6.48 (d, J = 5.9 Hz, 2H, $H_{Py'}$), 6.38 (d, J = 2.4 Hz, 2H, $H_{Im'}$), 5.59 (dd, J = 6.9, 2.3 Hz, 2H, NC*H*CH$_2$), 4.64 (ddd, J = 13.0, 7.0, 3.3 Hz, 2H, NCHC*H*$_2$), 4.56 (ddd, J = 13.0, 6.1, 2.4 Hz, 2H, NCHC*H*$_2$), 3.56 (dd, J = 6.0, 3.2 Hz, 2H, O*H*). ^{13}C{^{1}H} NMR (100.62 MHz, 295.5 K, CD_3CN): δ 209.92 (C_{Im}), 200.85 ($C_{Im'}$), 155.63 (C_{Py}), 155.32 ($C_{Py'}$), 154.13 (C_{Py}), 151.70 ($C_{Py'}$), 142.84 (C_{Py}), 140.98 ($C_{Py'}$), 126.48 (C_{Im}), 125.90 ($C_{Im'}$), 125.31 (C_{Py}), 124.03 ($C_{Py'}$), 121.61 (C_{Im}), 119.08 ($C_{Im'}$), 114.26 (C_{Py}), 112.76 ($C_{Py'}$), 75.16 (N*C*HCH$_2$),62.95 (NCH*C*H$_2$). MS-ESI (m/z): [**C3**–4CH$_3$CN–2PF$_6$]$^{2+}$ calcd: 533.04, found: 533.12. Anal. calcd for $C_{44}H_{44}F_{24}Fe_2N_{16}O_2P_4$ C 34.76, H 2.92, N 14.74. Found: C 34.46, H 3.13, N 14.24.

4.3.6. Ligand precursor P2a. P1 (500.0 mg, 0.8 mmol, 1.0 eq.) is dissolved in dried acetonitrile (3 mL) and hexanoyl chloride (224 μL, 1.6 mmol, 2.0 eq.) and pyridine (129 μL, 1.6 mmol, 2.0 eq.) are subsequently added. After stirring the reaction mixture at room temperature for 21 h the white precipitate is filtered off and the resulting solution is dried *in vacuo*. The resulting oily residue is redissolved in acetone (1 mL) and slowly added to a solution of ammonium hexafluorophosphate (260.8 mg, 1.6 mmol, 2.0 eq.) in water (3 mL) yielding a brown solution, which is subjected to reduced pressure until the acetone evaporates and a brown residue precipitates from the aqueous phase. After decantation and washing with water (3 mL) the oily residue is dissolved in acetone and precipitates by slow addition of diethyl ether. The off-white precipitate is isolated by filtration, washed with diethyl ether (5 mL) and dried *in vacuo* yielding **P2a** (471.5 mg, 0.65 mmol) in 82% yield.

^{1}H NMR (400.13 MHz, 295.1 K, DMSO-d_6): δ 10.43 (t, J = 1.6 Hz, 2H, H_{Im}), 8.76–8.68 (m, 4H, H_{Im} + H_{Py}), 8.35 (t, J = 2.0 Hz, 2H, H_{Im}), 8.33–8.25 (m, 2H, H_{Py}), 8.08 (dt, J = 8.3, 0.9 Hz, 2H, H_{Py}), 7.72 (ddd, J = 7.6, 4.8, 0.9 Hz, 2H, H_{Py}), 7.53 (t, J = 5.8 Hz, 1H, NC*H*CH$_2$), 5.21 (d, J = 5.8 Hz, 2H, NCHC*H*$_2$), 2.38 (t, J = 7.4 Hz, 2H, H_{Hex}), 1.48 (p, J = 7.3 Hz, 2H, H_{Hex}), 1.24–1.12 (m, 4H, H_{Hex}), 0.78 (t, J = 6.9 Hz, 3H, H_{Hex}). ^{13}C{^{1}H} NMR (100.62 MHz, 295.5 K, DMSO-d_6): δ 172.04 (*C*=O), 149.49 (C_{Py}), 145.95 (C_{Py}), 140.95 (C_{Py}), 136.78 (C_{Im}), 125.96 (C_{Py}), 122.33 (C_{Im}), 120.06 (C_{Im}), 114.50 (C_{Py}), 68.68 (N*C*HCH$_2$), 60.78

(NCHCH$_2$), 33.03 ($C_{2,\mathrm{Hex}}$), 30.49 ($C_{3,\mathrm{Hex}}$), 23.84 ($C_{4,\mathrm{Hex}}$), 21.76 ($C_{5,\mathrm{Hex}}$), 13.75 ($C_{6,\mathrm{Hex}}$). MS-ESI (m/z): [**P2a**–2PF$_6$]$^{2+}$ calcd: 216.11, found: 216.16. Anal. calcd for $C_{24}H_{28}N_6O_2P_2F_{12}$ C 39.90, H 3.91, N 11.63. Found: C 39.51, H 3.92, N 11.45.

4.3.7. Ligand precursor P2b. **P1** (1000.0 mg, 1.6 mmol, 1.0 eq.) is dissolved in dried acetonitrile (15 mL) and pyridine (387 μL, 4.8 mmol, 3.0 eq.) and benzoyl chloride (992 μL, 8.0 mmol, 5.0 eq.) are subsequently added under ice cooling. After stirring the reaction mixture at room temperature for 12 h the solvent is removed *in vacuo*. The resulting solid is dissolved in methanol (20 mL) and slowly added to a solution of ammonium hexafluorophosphate (239.4 mg, 3.2 mmol, 2.0 eq.) in water (5 mL). The white precipitate is isolated by filtration and washed with water (5 mL) and diethyl ether (5 mL) and dried *in vacuo* yielding **P2b** (571.3 mg, 0.78 mmol) in 49% yield.

^{1}H NMR (400.13 MHz, 295.1 K, DMSO-d_6): δ 10.53 (s, 2H, H_{Im}), 8.73 (s, 2H, H_{Im}), 8.71 (d, J = 4.7 Hz, 2H, H_{Py}), 8.42 (s, 2H, H_{Im}), 8.26 (t, J = 7.7 Hz, 2H, H_{Py}), 8.08 (d, J = 8.2 Hz, 2H, H_{Py}), 8.01 (d, J = 7.8 Hz, 2H, H_{Ph}), 7.70 (m, 4H, H_{Py} + H_{Ph} + NCHCH$_2$), 7.54 (t, J = 7.7 Hz, 2H, H_{Ph}), 5.44 (d, J = 5.3 Hz, 2H, NCHCH$_2$). ^{13}C{^{1}H} NMR (100.62 MHz, 295.5 K, DMSO-d_6): δ 164.73 (C═O), 149.48 (C_{Py}), 146.03 (C_{Py}), 140.92 (C_{Py}), 136.96 (C_{Im}), 134.10 (C_{Ph}), 129.69 (C_{Ph}), 128.90 (C_{Ph}), 128.48 (C_{Ph}), 125.91 (C_{Py}), 122.39 (C_{Im}), 120.08 (C_{Im}), 114.53 (C_{Py}), 68.98 (NCHCH$_2$), 61.81 (NCHCH$_2$). MS-ESI (m/z): [**P2b**–2PF$_6$]$^{2+}$ calcd: 219.09, found: 219.17. Anal. calcd for $C_{25}H_{22}N_6O_2P_2F_{12}$ C 41.22, H 3.04, N 11.54. Found: C 41.79, H 3.12, N 11.77.

4.3.8. Ligand precursor P2c. **P1** (500.0 mg, 0.8 mmol, 1.0 eq.) is dissolved in dried acetonitrile (5 mL) and nicotinoyl chloride (226.5 mg, 1.6 mmol, 2.0 eq.) and pyridine (129 μL, 1.6 mmol, 2.0 eq.) are subsequently added. After stirring the reaction mixture at room temperature for 17 h the white precipitate is filtered off and the filtrate is dried *in vacuo*. The oily residue is redissolved in acetone (1 mL) and slowly added to a solution of ammonium hexafluorophosphate (260.8 mg, 1.6 mmol, 2.0 eq.) in water (2 mL) yielding a brown solution, which is subjected to reduced pressure until the acetone evaporates and a brown residue precipitates from the aqueous phase. After decantation, the product is subsequently extracted from the residue with water by dissolving it in a mixture of acetone and water (1 : 1), evaporating the acetone and decanting the aqueous phase. The combined aqueous phases are dried *in vacuo* and the raw product is dissolved in acetone and precipitated by slow addition of dichloromethane. The light orange precipitate is isolated, washed with dichloromethane (5 mL) and dried *in vacuo* yielding **P2c** (257.6 mg, 0.35 mmol) in 44% yield.

^{1}H NMR (400.13 MHz, 295.1 K, DMSO-d_6): δ 10.50 (t, J = 1.6 Hz, 2H, H_{Im}), 9.19 (d, J = 2.2 Hz, 1H, H_{Nic}), 8.85 (dd, J = 4.9, 1.7 Hz, 1H, H_{Nic}), 8.73 (t, J = 2.0 Hz, 2H, H_{Im}), 8.71 (dd, J = 5.1, 1.7 Hz, 2H, H_{Py}), 8.40 (t, J = 1.9 Hz, 2H, H_{Im}), 8.36 (dt, J = 8.0, 2.0 Hz, 1H, H_{Nic}), 8.28 (td, J = 7.9, 1.9 Hz, 2H, H_{Py}), 8.08 (d, J = 8.3 Hz, 2H, H_{Py}), 7.71 (dd, J = 7.5, 4.9 Hz, 2H, H_{Py}), 7.67 (t, J = 5.0 Hz, 1H, NCHCH$_2$), 7.59 (dd, J = 8.0, 4.9 Hz, 1H, H_{Nic}), 5.44 (d, J = 5.0 Hz, 2H, NCHCH_2). ^{13}C{^{1}H} NMR (100.62 MHz, 295.5 K, DMSO-d_6): δ 163.87 (C═O), 154.18 (C_{Nic}), 150.54 (C_{Nic}), 149.49 (C_{Py}), 146.06 (C_{Py}), 140.93 (C_{Py}), 137.43 (C_{Nic}), 137.02 (C_{Im}), 125.91 (C_{Py}), 124.85 (C_{Nic}), 124.04 (C_{Nic}), 122.46 (C_{Im}), 120.05 (C_{Im}), 114.53 (C_{Py}), 68.97 (NCHCH$_2$), 62.15 (NCHCH$_2$). MS-ESI (m/z): [**P2c**–2PF$_6$]$^{2+}$ calcd: 219.59, found: 219.93. [**P2c**–PF$_6$]$^+$ calcd: 584.14, found: 584.04. Anal. calcd for $C_{24}H_{21}F_{12}FeN_7O_2P_2$ C 39.52, H 2.90, N 13.44. Found: C 38.95, H 3.00, N 13.17.

4.3.9. Complexes C2a–C2c. A solution of the respective ligand precursor **P2a–P2c** (0.07 mmol, 1.0 eq.) in acetonitrile (1.5 mL) is added to a frozen solution of [Fe{N(SiMe$_3$)$_2$}$_2$(THF)] (0.09 mmol, 1.3 eq.) in acetonitrile (1 mL) and after warming to room temperature it is stirred for 14 h. Subsequently the solvent is removed *in vacuo* and the residual solid is redissolved in acetonitrile. By addition of diethyl ether the solution is precipitated stepwise. The red product complexes **C2a–C2c** are washed with diethyl ether and dried *in vacuo*.

*4.3.9.1. Complex **C2a**.* ^{1}H NMR (400.13 MHz, 295.1 K, CD$_3$CN): δ 9.58 (dd, J = 5.3, 1.8 Hz, 2H, H_{Py}), 8.41–8.33 (m, 2H, H_{Py}), 8.31 (d, J = 2.2 Hz, 3H, H_{Im}), 8.07 (dt, J = 8.3, 1.0 Hz, 2H, H_{Py}), 7.93 (d, J = 2.5 Hz, 2H, H_{Im}), 7.78 (t, J = 6.4 Hz, 2H, H_{Py}), 7.43 (t, J = 5.5 Hz, 1H, NCHCH$_2$), 4.60 (d, J = 5.5 Hz, 2H, NCHCH_2), 2.29 (t, J = 7.4 Hz, 7H, H_{Alk}), 1.52 (tt, J = 7.3, 7.3 Hz, 2H, H_{Alk}), 1.34–1.19 (m, 4H, H_{Alk}), 0.86 (t, J = 7.0 Hz, 3H, H_{Alk}). ^{13}C{^{1}H} NMR (100.62 MHz, 295.5 K, CD$_3$CN): δ 217.50 (C_{Im}), 173.41 (C═O), 155.18 (C_{Py}), 153.78 (C_{Py}), 142.46 (C_{Py}), 126.58 (C_{Im}), 124.57 (C_{Py}), 120.33 (C_{Im}), 113.21 (C_{Py}), 74.09 (NCHCH$_2$), 67.98 (NCHCH$_2$), 34.22 ($C_{2,\mathrm{Hex}}$), 31.78 ($C_{3,\mathrm{Hex}}$), 25.02 ($C_{4,\mathrm{Hex}}$), 23.00 ($C_{5,\mathrm{Hex}}$), 14.19 ($C_{6,\mathrm{Hex}}$). MS-ESI (m/z): [**C2a**–2CH$_3$CN–2PF$_6$]$^{2+}$ calcd: 243.07, found: 243.53. Anal. calcd for $C_{28}H_{32}F_{12}FeN_8O_2P_2$: C 39.18, H 3.76, N 13.05. Found: C 39.07, H 3.78, N 12.85. Yield: 62%.

*4.3.9.2. Complex **C2b**.* ^{1}H NMR (400.13 MHz, 295.1 K, CD$_3$CN): δ 9.56 (dd, J = 5.3, 0.8 Hz, 2H, H_{Py}), 8.35 (ddd, J = 8.3, 7.5, 1.6 Hz, 2H, H_{Py}), 8.30 (d, J = 2.3 Hz, 2H, H_{Im}), 8.06 (dt, J = 8.3, 1.0 Hz, 2H, H_{Py}), 8.00 (d, J = 2.3 Hz, 2H, H_{Im}), 7.99–7.94 (m, 2H, H_{Ph}), 7.76 (ddd, J = 7.5, 5.4, 1.1 Hz, 2H, H_{Py}), 7.68–7.62 (m, 1H, H_{Ph}), 7.59 (t, J = 5.5 Hz, 1H, NCHCH$_2$), 7.53–7.47 (m, 2H, H_{Ph}), 4.83 (d, J = 5.5 Hz, 2H, NCHCH_2). ^{13}C{^{1}H} NMR (100.62 MHz, 295.5 K, CD$_3$CN): δ 217.66 (C_{Im}), 166.19 (C═O), 155.19 (C_{Py}), 153.75 (C_{Py}), 142.44 (C_{Py}), 134.90 (C_{Ph}), 130.59 (C_{Ph}), 129.89 (C_{Ph}), 126.67 (C_{Im}), 124.53 (C_{Py}), 120.37 (C_{Im}), 115.97 (C_{Ph}), 113.22 (C_{Py}), 74.14 (NCHCH$_2$), 68.89 (NCHCH$_2$). MS-ESI (m/z): [**C2b**–2CH$_3$CN–2 PF$_6$]$^{2+}$ calcd: 246.05, found: 246.23. Anal. calcd for $C_{29}H_{26}FeN_8O_2P_2F_{12}$: C 40.30, H 3.03, N 12.96. Found: C 39.85, H 3.06, N 12.35. Yield: 52%.

*4.3.9.3. Complex **C2c**.* ^{1}H NMR (400.13 MHz, 295.1 K, CD$_3$CN): δ 9.56 (d, J = 5.4 Hz, 2H, H_{Py}), 9.11 (s, 1H, H_{Nic}), 8.82 (d, J = 5.2 Hz, 1H, H_{Nic}), 8.48 (d, J = 8.0 Hz, 1H, H_{Nic}), 8.39–8.32 (m, 2H, H_{Py}), 8.30 (d, J = 2.3 Hz, 2H, H_{Im}), 8.07 (d, J = 8.2 Hz, 2H, H_{Py}), 8.02 (d, J = 2.3 Hz, 2H, H_{Im}), 7.75 (dd, J = 7.7, 5.2 Hz, 2H, H_{Py}), 7.73–7.67 (m, 1H, H_{Nic}), 7.58 (t, J = 5.8 Hz, 1H, NCHCH$_2$), 4.78 (d, J = 5.9 Hz, 2H, NCHCH_2). ^{13}C{^{1}H} NMR (100.62 MHz, 295.5 K, CD$_3$CN): δ 217.72 (C_{Im}), 165.23(C═O), 155.20 (C_{Nic}), 155.17 (C_{Py}), 153.77 (C_{Py}), 151.51 (C_{Nic}), 142.45 (C_{Py}), 138.15 (C_{Nic}), 126.66 (C_{Im}), 125.97 (C_{Nic}), 124.86 (C_{Nic}),

124.56 (C_{Py}), 120.43 (C_{Im}), 113.23 (C_{Py}), 73.96 (NCHCH$_2$), 69.06 (NCHCH$_2$). MS-ESI (m/z): [**C2c**–CH_3CN–$2PF_6$]$^{2+}$ calcd: 267.06, found: 267.43. Anal. calcd for $C_{24}H_{21}F_{12}FeN_7O_2P_2$ + HPF_6: C 33.25, H 2.59, N 12.47. Found: C 32.98, H 2.90, N 11.92. Yield: 76%.

4.3.10. Esterification of complex C2 by organic anhydrides. Method A. The respective organic acid (52.6 μmol, 2.0 eq.) is dissolved in trifluoroacetic anhydride (7.4 μL, 52.6 μmol, 2.0 eq.) and the mixture is stirred for 5 min before adding it to a solution of **C2** (20.0 mg, 26.3 μmol, 1.0 eq.) in 0.5 mL acetonitrile. In case of trifluoroacetic acid, the anhydride is added directly to the complex solution. After a reaction time of 1–20 h diethyl ether is slowly added to precipitate the product complexes, which are isolated by filtration.

Method B. The respective organic anhydride (28.9 μmol, 1.1 eq.) and **C2** (20.0 mg, 26.3 μmol, 1.0 eq.) are dissolved in 1.0 mL acetonitrile and subsequently diisopropylethylamine (4.9 μL, 28.9 μmol, 1.1 eq.) is added. After a reaction time of 3 h diethyl ether is slowly added to precipitate the product complexes, which are isolated by filtration.

*4.3.10.1. Complex **C2d**.* ^{1}H NMR (400.13 MHz, 295.1 K, CD_3CN): δ 9.58 (ddd, J = 5.4, 1.6, 0.7 Hz, 2H, H_{Py}), 8.37 (ddd, J = 8.2, 7.5, 1.6 Hz, 2H, H_{Py}), 8.32 (d, J = 2.3 Hz, 2H, H_{Im}), 8.07 (dt, J = 8.4, 1.0 Hz, 2H, H_{Py}), 7.93 (d, J = 2.3 Hz, 2H, H_{Im}), 7.79 (ddd, J = 7.5, 5.4, 1.2 Hz, 2H, H_{Py}), 7.58 (t, J = 5.6 Hz, 1H, NC*H*CH$_2$), 4.83 (d, J = 5.5 Hz, 2H, NCHC*H*$_2$). ^{13}C{^{1}H} NMR (100.62 MHz, 295.5 K, CD_3CN): δ 217.97 (C_{Im}), 156.95 (q, J = 43.2 Hz, *C*=O), 155.05 (C_{Py}), 153.74 (C_{Py}), 142.48 (C_{Py}), 126.51 (C_{Im}), 124.62 (C_{Py}), 120.51 (C_{Im}), 115.28 (q, J = 284.6 Hz, *C*F$_3$), 113.23 (C_{Py}), 73.03 (N*C*HCH$_2$), 71.09 (NCH*C*H$_2$). MS-ESI (m/z): [**C2d**–$2CH_3CN$–$2PF_6$]$^{2+}$ calcd: 242.03, found: 242.63. Anal. calcd for $C_{24}H_{21}F_{15}FeN_8O_2P_2$: C 33.67, H 2.47, N 13.09. Found: C 33.66, H 2.55, N 12.81. Yield: 98%.

Conflicts of interest

There are no conflicts to declare.

Acknowledgements

The authors appreciate financial support by the Fonds der Chemischen Industrie (FCI). Peter Gänsheimer is acknowledged for his valuable experimental contributions.

References

1 W. A. Herrmann, M. Elison, J. Fischer, C. Köcher and G. R. J. Artus, *Angew. Chem., Int. Ed. Engl.*, 1995, **34**, 2371–2374.
2 W. A. Herrmann and C. Köcher, *Angew. Chem., Int. Ed. Engl.*, 1997, **36**, 2162–2187.
3 F. Glorius, in *N-Heterocyclic Carbenes in Transition Metal Catalysis*, ed. F. Glorius, Springer, Berlin, Heidelberg, Germany, 2007, pp. 1–20.
4 L. Cavallo and C. S. J. Cazin, in *N-Heterocyclic Carbenes in Transition Metal Catalysis and Organocatalysis*, ed. C. S. J. Cazin, Springer, Dordrecht, The Netherlands, 2011, pp. 1–22.
5 P. de Frémont, N. Marion and S. P. Nolan, *Coord. Chem. Rev.*, 2009, **253**, 862–892.
6 F. E. Hahn and M. C. Jahnke, *Angew. Chem., Int. Ed.*, 2008, **47**, 3122–3172.
7 M. Poyatos, J. A. Mata and E. Peris, *Chem. Rev.*, 2009, **109**, 3677–3707.
8 J. A. Mata, M. Poyatos and E. Peris, *Coord. Chem. Rev.*, 2007, **251**, 841–859.
9 R. Corberán, E. Mas-Marzá and E. Peris, *Eur. J. Inorg. Chem.*, 2009, **2009**, 1700–1716.
10 R. Zhong, A. C. Lindhorst, F. J. Groche and F. E. Kühn, *Chem. Rev.*, 2017, **117**, 1970–2058.
11 E. Mas-Marzá, M. Poyatos, M. Sanaú and E. Peris, *Organometallics*, 2004, **23**, 323–325.
12 E. Mas-Marzá, M. Sanaú and E. Peris, *J. Organomet. Chem.*, 2005, **690**, 5576–5580.
13 M. Viciano, E. Mas-Marzá, M. Poyatos, M. Sanaú, R. H. Crabtree and E. Peris, *Angew. Chem., Int. Ed.*, 2005, **44**, 444–447.
14 O. Kühl, *Germany Pat*, WO2012034880A1, 2012.
15 R. Zhong, A. Pöthig, S. Haslinger, B. Hofmann, G. Raudaschl-Sieber, E. Herdtweck, W. A. Herrmann and F. E. Kühn, *ChemPlusChem*, 2014, **79**, 1294–1303.
16 R. Zhong, A. Pöthig, D. C. Mayer, C. Jandl, P. J. Altmann, W. A. Herrmann and F. E. Kühn, *Organometallics*, 2015, **34**, 2573–2579.
17 J. Rieb, B. Dominelli, D. Mayer, C. Jandl, J. Drechsel, W. Heydenreuter, S. A. Sieber and F. E. Kühn, *Dalton Trans.*, 2017, **46**, 2722–2735.
18 R. Puerta-Oteo, M. Hölscher, M. V. Jiménez, W. Leitner, V. Passarelli and J. J. Pérez-Torrente, *Organometallics*, 2017, DOI: 10.1021/acs.organomet.7b00509.
19 K. Riener, S. Haslinger, A. Raba, M. P. Högerl, M. Cokoja, W. A. Herrmann and F. E. Kühn, *Chem. Rev.*, 2014, **114**, 5215–5272.
20 V. Charra, P. de Frémont and P. Braunstein, *Coord. Chem. Rev.*, 2017, **341**, 53–176.
21 S. Haslinger, A. Raba, M. Cokoja, A. Pöthig and F. E. Kühn, *J. Catal.*, 2015, **331**, 147–153.
22 Ö. Karaca, M. R. Anneser, J. W. Kück, A. C. Lindhorst, M. Cokoja and F. E. Kühn, *J. Catal.*, 2016, **344**, 213–220.
23 J. W. Kück, A. Raba, I. I. E. Markovits, M. Cokoja and F. E. Kühn, *ChemCatChem*, 2014, **6**, 1882–1886.
24 A. C. Lindhorst, J. Schütz, T. Netscher, W. Bonrath and F. E. Kühn, *Catal. Sci. Technol.*, 2017, **7**, 1902–1911.
25 A. Raba, M. Cokoja, W. A. Herrmann and F. E. Kühn, *Chem. Commun.*, 2014, **50**, 11454–11457.
26 A. Raba, M. Cokoja, S. Ewald, K. Riener, E. Herdtweck, A. Pöthig, W. A. Herrmann and F. E. Kühn, *Organometallics*, 2012, **31**, 2793–2800.

27 D. T. Weiss, P. J. Altmann, S. Haslinger, C. Jandl, A. Pöthig, M. Cokoja and F. E. Kühn, *Dalton Trans.*, 2015, **44**, 18329–18339.
28 Z. Lu, S. A. Cramer and D. M. Jenkins, *Chem. Sci.*, 2012, **3**, 3081–3087.
29 J. M. Smith and J. R. Long, *Inorg. Chem.*, 2010, **49**, 11223–11230.
30 Z. X. Xi, X. M. Zhang, W. Z. Chen, S. Z. Fu and D. Q. Wang, *Organometallics*, 2007, **26**, 6636–6642.
31 D. Christine, F. Rominger and D. Kunz, *Dalton Trans.*, 2009, **35**, 7152–7167.
32 J. C. Garrison and W. J. Youngs, *Chem. Rev.*, 2005, **105**, 3978–4008.
33 A. A. Danopoulos, P. Braunstein, N. Stylianides and M. Wesolek, *Organometallics*, 2011, **30**, 6514–6517.
34 K. V. S. Ranganath, S. Onitsuka, A. K. Kumar and J. Inanaga, *Catal. Sci. Technol.*, 2013, **3**, 2161–2181.
35 P. J. Altmann and A. Pöthig, *Angew. Chem., Int. Ed.*, 2017, **56**, 15733–15736.
36 G. Kortüm, W. Vogel and K. Andrussow, *Pure Appl. Chem.*, 1960, **1**, 187–536.
37 B. García, S. Ibeas and J. M. Leal, *J. Phys. Org. Chem.*, 1996, **9**, 593–597.
38 D. T. Weiss, M. R. Anneser, S. Haslinger, A. Pöthig, M. Cokoja, J.-M. Basset and F. E. Kühn, *Organometallics*, 2015, **34**, 5155–5166.
39 M. R. Anneser, S. Haslinger, A. Pöthig, M. Cokoja, J.-M. Basset and F. E. Kühn, *Inorg. Chem.*, 2015, **54**, 3797–3804.
40 S. Haslinger, J. W. Kück, E. M. Hahn, M. Cokoja, A. Pöthig, J. M. Basset and F. E. Kühn, *Inorg. Chem.*, 2014, **53**, 11573–11583.
41 I. Klawitter, M. R. Anneser, S. Dechert, S. Meyer, S. Demeshko, S. Haslinger, A. Pöthig, F. E. Kühn and F. Meyer, *Organometallics*, 2015, **34**, 2819–2825.
42 J. Heinze, *Angew. Chem.*, 1984, **96**, 823–840.
43 S. Haslinger, A. C. Lindhorst, J. W. Kück, M. Cokoja, A. Pöthig and F. E. Kühn, *RSC Adv.*, 2015, **5**, 85486–85493.
44 D. Astruc, *Acc. Chem. Res.*, 1997, **30**, 383–391.
45 S. Barlow and D. O'Hare, *Chem. Rev.*, 1997, **97**, 637–670.
46 L. Mercs, A. Neels, H. Stoeckli-Evans and M. Albrecht, *Dalton Trans.*, 2009, **35**, 7168–7178.
47 B. R. Serr, K. A. Andersen, C. M. Elliott and O. P. Anderson, *Inorg. Chem.*, 1988, **27**, 4499–4504.
48 A. Raba, M. R. Anneser, D. Jantke, M. Cokoja, W. A. Herrmann and F. E. Kühn, *Tetrahedron Lett.*, 2013, **54**, 3384–3387.
49 M. M. Olmstead, P. P. Power and S. C. Shoner, *Inorg. Chem.*, 1991, **30**, 2547–2551.
50 N. G. Connelly and W. E. Geiger, *Chem. Rev.*, 1996, **96**, 877–910.
51 *APEX 2, version 2008.4*, Bruker AXS Inc., Madison, WI, USA, 2008.
52 *APEX 3, version 2015.5-2*, Bruker AXS Inc., Madison, WI, USA, 2015.
53 *SAINT and SADABS, version 7.56a and 2008/1*, Bruker AXS Inc., Madison, WI, USA, 2008.
54 G. M. Sheldrick, *SHELXL-2014*, University of Göttingen, Göttingen, Germany, 2014.
55 C. B. Hübschle, G. M. Sheldrick and G. Dittrich, *J. Appl. Crystallogr.*, 2011, **44**, 1281–1284.
56 G. M. Sheldrick, *SHELXL-97*, University of Göttingen, Göttingen, Germany, 1998.
57 A. J. Wilson, *International Tables for Crystallography. Vol. C, Tables 6.1.1.4 (pp. 500-502), 4.2.6.8 (pp. 219-222), and 4.2.4.2 (pp. 193-199)*, Kluwer Academic Publishers, Dordrecht, The Netherlands, 1992.
58 A. L. Spek, *PLATON, A Multipurpose Crystallographic Tool*, Utrecht University, Utrecht, The Netherlands, 2010.